Desalination and Water Treatment
www.deswater.com

doi: 10.5004/dwt.2021.26505

210 (2021) 316–329
January

Investigation of adsorption activity of poly(acrylamide–styrene)/bentonite nanocomposite for efficient removal of manganese ions from aqueous solution

Amir Ebrahim Baradaran Mahdavi[a,b], Ebrahim Panahpour[b,*], Roozbeh Javad Kalbasi[c,*], Ali Gholami[b]

[a]*Department of Soil Science, Khouzestan Science and Research Branch, Islamic Azad University, Ahvaz, Iran, email: amirmahdavi2000@gmail.com*
[b]*Department of Soil Science, Ahvaz Branch, Islamic Azad University, Ahvaz, Iran, emails: e.panahpour@gmail.com (E. Panahpour), ali.gholami54@gmail.com (A. Gholami)*
[c]*Faculty of Chemistry, Kharazmi University, Tehran, Iran, email: rkalbasi@khu.ac.ir*

Received 4 January 2020; Accepted 25 August 2020

ABSTRACT

Removal of heavy metals which are produced from industrial and agricultural processes is essential due to their adverse effects on the environment. In the present work, polyacrylamide–polystyrene/bentonite nanocomposite was easily synthesized through in situ polymerization and used for the removal of manganese ions from aqueous solutions. The properties of the nanocomposite synthesized by field emission scanning electron microscopy, transmission electron microscopy, Fourier transformation infrared spectroscopy, X-ray diffraction, Brunauer–Emmett–Teller and thermogravimetric analysis techniques. Then, at the optimum values (pH = 6, contact time = 12 h, adsorbent value = 5 g and manganese ion concentration = 150 ppm), the manganese ions (cations) in the solution were adsorbed by the nanocomposite adsorbent polyacrylamide–polystyrene/bentonite and the amount of absorption was measured by atomic absorption, which was 84.2% and 82.1% for analyze and real sample, respectively.

Keywords: Heavy metal; Nanocomposite; Bentonite; Polyacrylamide; Adsorption; Adsorbent

1. Introduction

Heavy metals in waste waters produced by industries are regarded a global concern [1–3]. At low concentrations, manganese sustains various physiological processes in the human body, found in a variety of dietary sources. Indeed, excessive manganese accumulation in the central nervous system (CNS) can cause a phenomenon known as manganese, which resembles idiopathic Parkinson's disease in its clinical features and results in adverse neurological effects both in laboratory animals and humans. Overexposure and inhalation of manganese can also bring about symptoms such as pneumonia, decreased libido and sperm damage. Manganese has a toxic effect on the CNS. At high exposure levels, there are two types of effects. In the acute phase, psychiatric symptoms dominate ("manganese madness") with hallucinations, emotional lability and compulsive and aberrant behavior. Later, there appear neurological symptoms with muscular weakness, impaired speech, headache, clumsiness, tremor, mild rigidity and hypokinetic (mask-like) facial expressions. These symptoms are similar to those seen in Parkinson's disease, and they are typical of chronic manganese poisoning [4–7]. Hence, we need to thoroughly know the effects of manganese on crop growth and ultimate yield levels [8].

Different methods in previous studies were adopted to purify and recover manganese ions from wastewater [9–11]; however, adsorption is selected as the most beneficial and successful technique due to its high efficiency and effective handling, availability of different adsorbents and

* Corresponding authors.

reasonable cost [12–14]. In this study, nanocomposite polyacrylamide–polystyrene/bentonite was synthesized through in-situ polymerization, in which the layered silicate is swollen within the monomer solution; therefore, the polymer is formed between the intercalated sheets. Polymer–bentonite composites have combined properties in comparison with individual bentonite and polymer; these compounds have better thermal and mechanical properties, and porosity. Functional groups are able to improve metal adsorption properties of the polymer–bentonite composites [15–17]. Nowadays, polymeric adsorbents are considered as potential alternatives to traditional adsorbents because of their vast surface area, adjustable surface chemistry, pore size distribution, qualified mechanical rigidity and easy regeneration under mild conditions [18,19]. Surprisingly, polymeric adsorbents were very effective in removing various pollutants. Organic polymers such as polystyrene, polyaniline, bearing multi-functional groups such as –OH and $–NH_2$, are able to remove heavy metals from water through the process of precipitation [20–23].

Although the ions of heavy metals were not adsorbed well on the surface of bentonite minerals directly and the adsorption takes place in an ion-exchange mechanism due to low cation exchange capacity of the untreated bentonite, bentonite minerals are potentially good adsorbents [1,24]. However, they are not sufficient for large-scale applications due to the aforementioned restriction in the cation exchange. Therefore, chemical or physical modification can be applied to the bentonite surface and layers bearing certain functional groups with donor atoms such as oxygen, nitrogen and sulfur. Yet, there is still one problem in achieving high selectivity which will be solved using "molecular imprinting" technique. In this technique, the template of a molecule in an organic polymer was created, and was used to recognize other molecules with the same template [25,26].

The development of nanotechnology improves the treatment efficiency of nanocomposite, as a matrix, and the adsorption selectivity of heavy metal ions through both ion exchange and chelation owing to their carboxyl and amide groups [27].

2. Materials and methods

2.1. Materials

The materials for chemical reactions including acrylamide, benzoyl peroxide, styrene, tetrahydrofuran (THF), acetic acid, sodium acetate, buffers 2 to 7, hydrochloric acid, sodium chloride, silver nitrate, manganese nitrate and ethanol were prepared from Sigma-Aldrich (China), Merck (Canada), Fluka (Germany) companies Bentonite was prepared from the Mehrijan-Salafchegan mine of Iran.

2.2. Preparation of polyacrylamide–polystyrene/bentonite nanocomposite

After preparation of bentonite, to synthesize the nanocomposite, we performed in situ polymerization. For this purpose, 1 g of the processed bentonite, 1 g of acrylamide (0.908 mmol) and 14 mL of THF (tetrahydrofuran) were added to a round-bottom flask, and the resulting mixture was mixed under reflux conditions at 90°C for 3 h. Once the obtained mixture was cooled down, 0.1 g of benzoyl peroxide and 10 mol.% of polystyrene were added to it and the resulting mixture was subjected to reflux conditions while being mixed by magnetic stirrer. Next, the resulting creamy-colored mixture was filtered, and the precipitate on the filter was washed several times by THF and finally dried at room temperature.

2.3. Characterization methods

Characterization of the nanocomposite was carried out by field emission scanning electron microscopy (FE-SEM model MIRA3TESCAN-XMU), X-ray diffraction (XRD model Philips TW3714, Amsterdam, Netherlands), specific surface area (Brunauer–Emmett–Teller BET model Belsorp mini II), Fourier transformation infrared spectroscopy (FT-IR model PerkinElmer Spectrum 65, USA) and transmission electron microscopy (TEM model Philips CM30, Amsterdam, Netherlands, electron microscope of the powdered sample mixed with ethanol, deposited on a copper grid and coated with carbon). Thermal gravimetric analysis was carried out by thermogravimetric analysis (TGA model PerkinElmer TGA7, USA). The amount of adsorbed ions from aqueous solution after extraction from the sample was measured by flame atomic adsorption spectroscopy atomic absorption (AA model PerkinElmer AAnalyst 300, USA) with different parameters for manganese (λ (wavelength) = 279.5 nm, slit = 0.2 nm, mA (mili Amper) = 30).

2.4. Adsorption experiments

Several effective factors on the adsorption process including pH, initial concentration, contact time and adsorbent dosage were studied.

All sorption experiments were conducted by the batch equilibration method. First, a stock solution with 1,000 mg/L of manganese was prepared in 1,000 mL of double distilled water. Next, the solution was diluted appropriately with a buffer to obtain the expected initial concentration in the adsorption study. In the initial conditions, 10 g adsorbents were added to a conical flask containing 1,000 mL of 10 mg/L of manganese as the initial concentration. The adsorption experiments were carried out at pH 6 under room temperature and the agitation speed of 300 rpm. After 6 h of adsorption, the reaction mixture was filtered and the filtrate was analyzed for non-adsorbed manganese to optimize conditions for manganese removal. Also, to measure the adsorption capacity of nanocomposite, the adsorption reactions were conducted at wide pH range (pH 2–7), contact time (2–24 h), initial concentration (10–200 mg/L) and adsorbent dose (5–15 g).

The manganese ion percentage removal was calculated by Eq. (1):

$$\text{Removal efficiency} = \frac{C_0 - C_e}{C_0} \times 100 \quad (1)$$

The adsorption capacity may be estimated using the following equation:

$$\text{Sorption capacity} = \frac{\left(C_0 - C_e\right)V}{m} \times 100 \quad (2)$$

where q_e is the adsorption capacities of adsorbents (mg Mn ion/g adsorbent), V is the volume of manganese ions solution (L), C_0 is the initial concentration of manganese ions before adsorption (mg/L), m is the weight of adsorbent (g) and C_e is the final concentration of manganese ions after adsorption (mg/L) [28].

2.5. Adsorption kinetics

The Lagergren's pseudo-first-order and pseudo-second-order kinetic models were employed to present the adsorption [29,30]. Lagergren's pseudo-first-order kinetic model is often calculated by the following equation:

$$\ln(q_e - q_t) = \ln q_e - kt \tag{3}$$

where q_e and q_t signify the amount of manganese adsorbed (mg/g) at the equilibrium and at any time t, and k is the rate constant (1/min). The levels of q_e and k can be determined from the linear plot of:

$$\ln\left(q_e - q_t\right) \text{vs. } t \tag{4}$$

The pseudo-second-order kinetic model is defined as:

$$\frac{t}{q_t} = \frac{1}{k_2 q_e^2} + \frac{t}{q_e} \tag{5}$$

where q_t and q_e are the amount of ion adsorbed at time t and at equilibrium (mg/g) and k_2 (g/mg min) is the pseudo-second-order rate constant for the adsorption process. From the intercept and the slope of the linear plot of t/q_t against t, constants can be determined based on experimental data.

2.6. Adsorption isotherms

Adsorption isotherm was carried out with five different initial concentrations (10–200 mg/L) of manganese. The most widely used isotherms, Langmuir and Freundlich models were applied to define the adsorption characteristics of nanocomposite for the removal of manganese from aqueous solution. The linear form of isotherm is calculated by Eqs. (6) and (7).

Langmuir isotherm [31,32]:

$$\frac{C_e}{q_e} = \frac{k_L}{q_m} + \frac{C_e}{q_m} \tag{6}$$

Freundlich isotherm:

$$\log q_e = \log k_f + \frac{1}{n}\left(\log C_e\right) \tag{7}$$

In this equation, q_e is the amount of manganese adsorbed per unit weight of the sorbent (mg/g), C_e is the equilibrium concentration of manganese in the solution (mg/L), k_f is the adsorption capacity and $1/n$ is considered as the adsorption intensity. q_m is the amount of adsorbent at the complete monolayer coverage (mg/g), which gives the maximum sorption capacity of sorbent, and K_L (mg/L) is Langmuir isotherm constant related to the energy of adsorption. The key characteristics of the Langmuir isotherm can be described in terms of the dimensionless constant separation factor or equilibrium parameter, R_L by Eq. (8) [33].

$$R_L = \frac{1}{1 + k_L C_0} \tag{8}$$

where C_0 (mg/L) is the initial manganese ions concentration.

3. Results and discussion

3.1. Characterization of polyacrylamide–polystyrene/bentonite nanocomposite

3.1.1. X-ray diffraction

The crystal lattice spacing can be measured through the diffraction angle (2θ). The interlayer spacing for bentonite was 1 nm. After the synthesis of nanocomposites, the diffraction peaks shift to the lower angles determining the interlayer distance of polyacrylamide ranging from 1 to 2–3 nm. In the PAA.B nanocomposite, the d001 diffraction peak on the XRD pattern disappeared (Fig. 1),

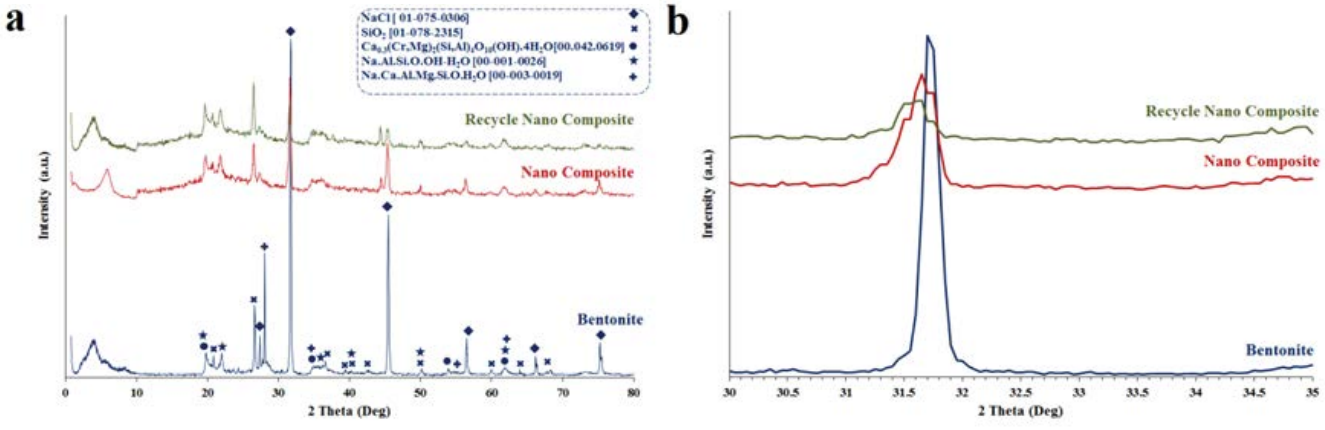

Fig. 1. (a) X-ray diffraction pattern of bentonite alone, PAA.B nanocomposite and PAA.B nanocomposite recovered at 2θ = 0–80 and (b) bentonite alone, polyacrylamide-PAA.B and PAA.B nanocomposite recovered at 2θ = 30–35.

which proves that the layered structure in the clay is completely demolished by in situ polymerization and that the nanocomposite is exfoliated. The XRD results showed clear differences in the crystalline structure of the nanocomposites. This also emphasized the importance of the polyacrylamide step to prepare exfoliated clay/polymer nanocomposite. It also highlights the role of the NH_2 group in confining the polymerization process to the interlayer spacing of the clay in which polyacrylamide has happened. If a standard micro composite was formed, that is a polymer coating stacked lamellar sheets, no exfoliated clay and thus the loss of d001 peak would have been recorded [34,35]. In the XRD pattern, PAA.B nanocomposite was observed at (2θ = 15–30) some amorphous phase. In addition, the displacement of the PAA.B nanocomposite spectra and the recovered sample from about 2θ = 31.8 to about 2θ = 31.4 indicate the placement of polymer strands between the bentonite layers.

3.1.2. Scanning electron microscopy

In Fig. 2, SEM images of PAA.B nanocomposite are shown. As shown in Fig. 2, the particle size is less than 200 nm. This shows the confirmation of the nanostructure. As can be seen in Fig. 2, the structure of bentonite is altered and the surface of the bentonite is evidently porous in nature before the synthesis of nanocomposite. The figure shows a massive layered structure with some large flakes and some interlayer spaces. It is evident that the interlayer spaces of clay are expanded indicating polyacrylamide being assembled on nanoparticles between the clay layers [36,37]. The small particle size and the porous structure provide a good adsorption capacity for manganese.

3.1.3. Transmission electron microscopy

In Figs. 3a and b, we can detect a more compact structure than the bentonite, and that the average of interlayer

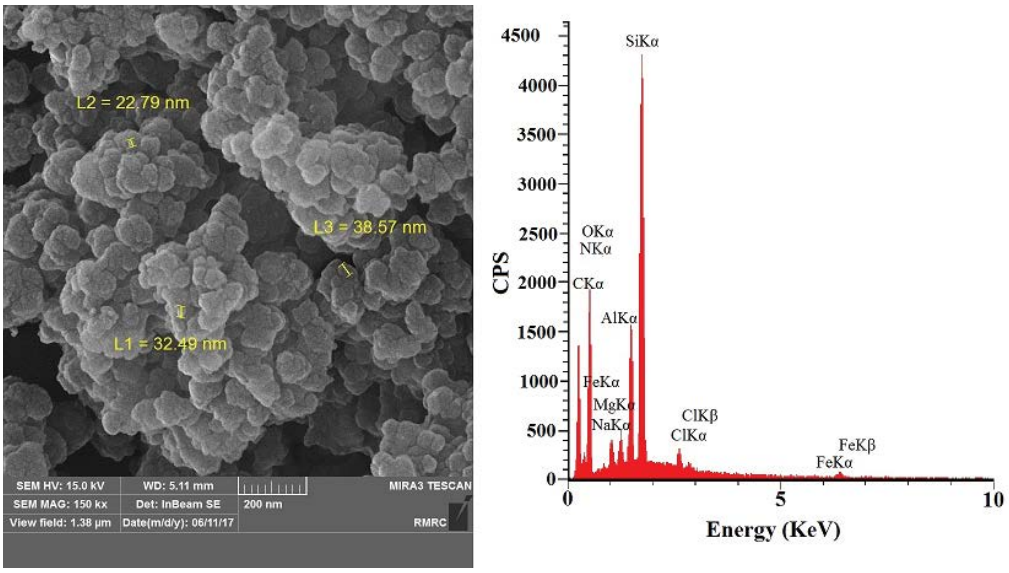

Fig. 2. Scanning electron microscope image of PAA.B nanocomposite.

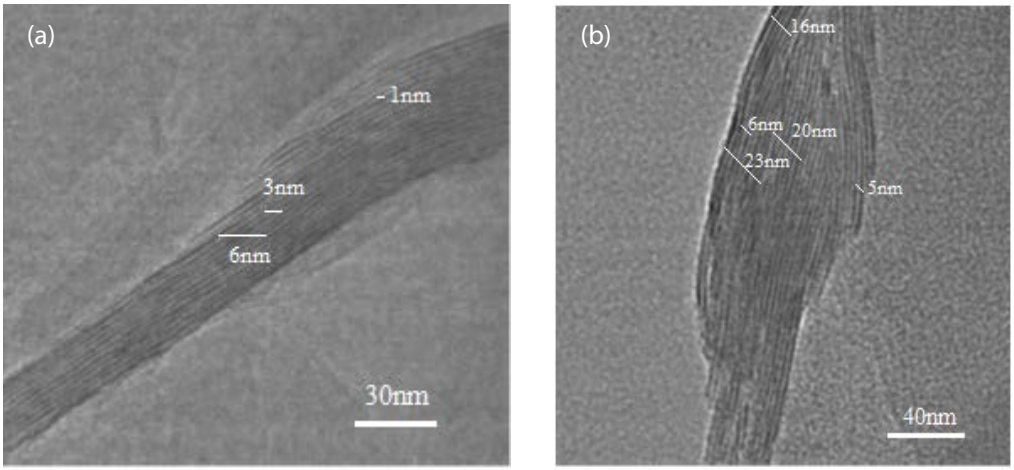

Fig. 3. TEM image of (a) bentonite and (b) PAA.B nanocomposite.

spaces of the PAA.B nanocomposite matches the distances determined by XRD (see previous section). Fig. 3a displays the TEM images related to the processed bentonite. In this image, the bentonite sample can be seen with a layered structure and interlayer distances of around 1–2 nm.

TEM image of PAA.B nanocomposite is displayed in Fig. 3b, which demonstrates the placement of polymer fibers among the interlayer distances of bentonite in the nanocomposite. It also shows the layered structure of bentonite. In this image, the size of interlayer distances is around 2–3 nm. Elevated interlayer distances suggest the placement of polymer fibers among the bentonite layers [38,39].

3.1.4. Fourier transformation infrared spectroscopy

FT-IR test was performed to identify the peaks of the products. In Fig. 4, FT-IR spectra in the range of 400–3,950 cm^{-1} are assigned for bentonite and in the range of 0–4,000 cm^{-1} for PAA.B, respectively. The bentonite peaks are as follows: broad and wide band in the area of 3,437 cm^{-1} region of water –OH and the hydroxyl group bonded (Si–OH) and the peaks of the 1,222; 1,172; 1,049 and 881 cm^{-1} regions are stretching and tensile vibrations of Si–O–Si and Si–O–Al and peaks in 1,450–1,600 cm^{-1} are stretching vibrations of C=C of aromatic styrene loops and peaks in the 3,200 and 3,400 cm^{-1} are stretching vibrations of NH_2 groups of polyacrylamides and peaks in 1,428 cm^{-1} are C–N bond polymer and hydroxides of bentonite surface. Peak in the 1,660 cm^{-1} region is the stretching vibrations of the carbonyl polyacrylamide group and that in the 2,942 cm^{-1} region is related to C–H, which is the aliphatic stretching of polyacrylamide and in the 1,030 cm^{-1} region is the stretching vibration of Si–O–Si bentonite bond [40,41].

3.1.5. Investigation of the isothermal graph of nitrogen adsorption/desorption

Fig. 5 shows the isothermal graph of polyacrylamide–polystyrene/bentonite adsorption/desorption. The specific surface area is determined according to this graph. The curve changes in Fig. 5 show the nanoscale porosity within the nanocomposite.

The specific surface area of most nanocomposite compounds is calculated using the BET method. This method is based on the single-layer nitrogen gas coated on the inner wall of the cavities and layers based on the measurement of the volume of nitrogen gas absorbed/desorbed by the surface of the material. While using this method, the points between P/P_0 = 0.01–0.2 are used because this region corresponds to the single-layer adsorption (Eq. (9)).

$$\frac{1}{\left[V_a\left(P_0/P-1\right)\right]}=\frac{C-1}{V_mC\left(P/P_0\right)}+\frac{1}{V_mC} \tag{9}$$

where P is partial pressure of gas adsorbed in equilibrium, P_0 denotes partial pressure of gas adsorbed under STP conditions, V_a represents the volume of gas adsorbed under STP conditions, V_m is the volume of adsorption gas under STP conditions for producing a single layer on sample surface and C represents the constant coefficient related to the adsorption enthalpy of adsorbed gas.

$$V_m=\frac{1}{A}+I \tag{10}$$

$$C=1+\frac{A}{I} \tag{11}$$

where I is the y-intercept of the BET diagram and A is the slope of BET diagram.

The S_{BET}'s specific surface area is calculated in Eq. (12):

$$S=\frac{V_m\left(N\right)a}{m\left(22,400\right)} \tag{12}$$

where N is the Avogadro number, a is the effective cross-section of the adsorbed molecule and m is the sample mass tested [42,43].

In Fig. 6, the BET measurement is observed for polyacrylamide–polystyrene/bentonite nanocomposite. In this figure, the specific surface area and the parameters A, I and C can be calculated.

The Kelvin equation in the BJH method is employed to determine the size, diameter, volume and regional distribution of the holes by the pore filling method in Figs. 7 and 8.

$$\ln\frac{p}{p_0}=2\gamma\frac{V_m}{rRT} \tag{13}$$

where p is actual vapor pressure, p_0 is saturation vapor pressure, γ is surface stress, r is radius of droplet, R is global gas constant and T is absolute temperature (K).

The surface area covered is calculated using the area occupied by a nitrogen molecule. The results of the nitrogen adsorption/desorption isothermal graphs and BJH and BET related to polyacrylamide–polystyrene/bentonite nanocomposite are displayed in Table 1.

According to S_{BET}, V_p and D of bentonite, which are 22.25 m^2/g, 0.016 cm^3/g and 29.6 nm, the results of the proposed nanocomposite show an acceptable increase in the surface, volume and size of the cavities.

3.1.6. Thermogravimetric analysis

Thermal analysis, which measures the mass of a sample over time by changing the temperature, is employed to calculate the heat-changing properties of materials such as dimension, mass, state and mechanical behavior. It is an analytical technique that uses volatile components to monitor the thermal stability of a substance as well as its body by monitoring the weight change.

In Fig. 9, the heat analysis diagram on processed bentonite and polyacrylamide–polystyrene/bentonite composite is provided.

Based on the analysis of the processed bentonite, the first weight loss step, which is estimated to be about 5% (at temperatures below 100°C), belongs to the water molecules absorbed by bentonite.

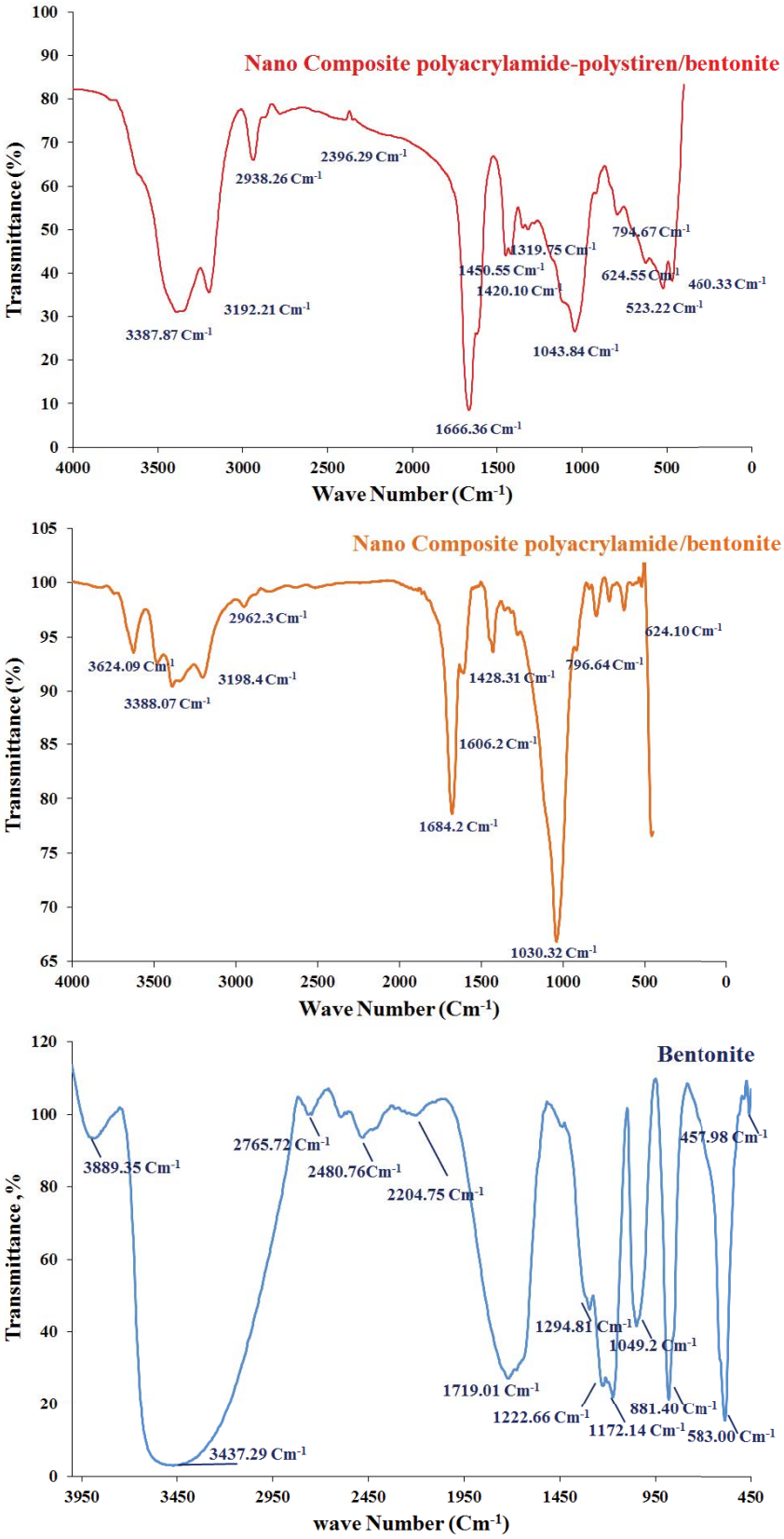

Fig. 4. Infrared spectra of PAA.B nanocomposite and Bentonite.

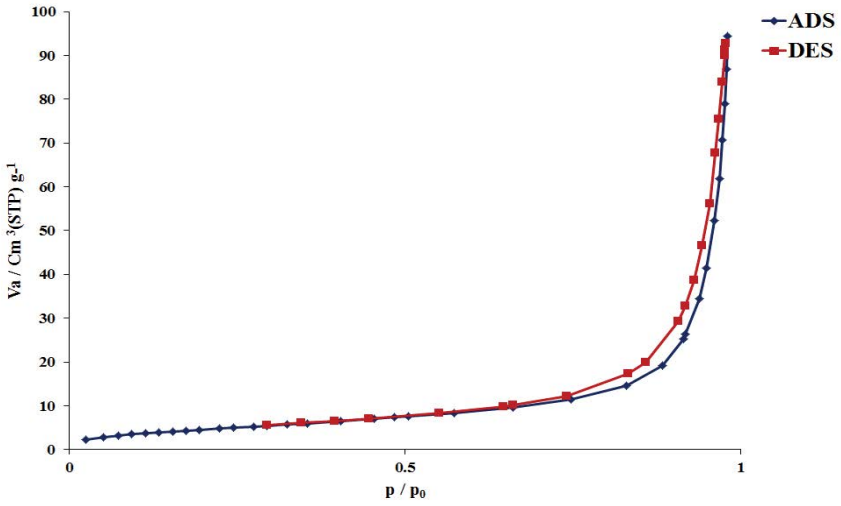

Fig. 5. Isothermal graph of polyacrylamide–polystyrene/bentonite adsorption/desorption.

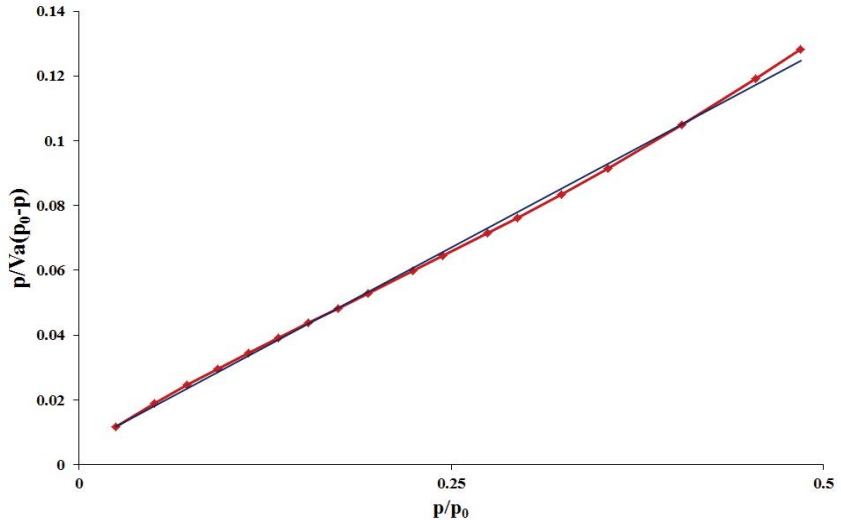

Fig. 6. BET of polyacrylamide–polystyrene/bentonite nanocomposite.

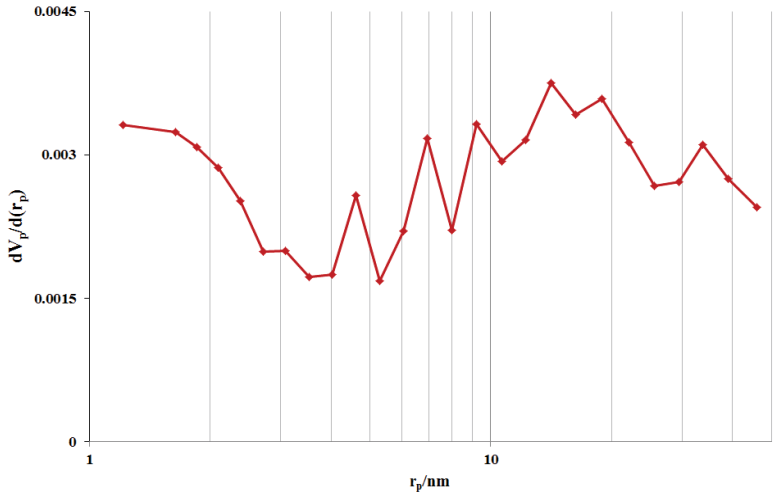

Fig. 7. BJH adsorption.

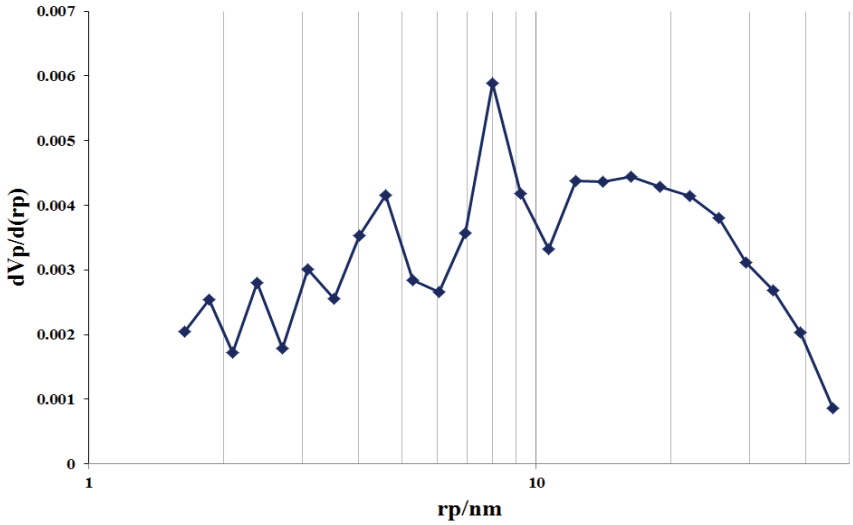

Fig. 8. BJH despondent.

Table 1
Nitrogen adsorption–desorption analysis of polyacrylamide–polystyrene/bentonite nanocomposite

S_{BET} (m^2/g)	28
D (nm)	32.5
V_p (cm^3/g)	0.14
S_{lang} (m^2/g)	26.8
$S_{mp\text{-}plot}$ (m^2/g)	22.8
d_p (nm)	2
$S_{T\text{-}plot}$ (m^2/g)	49.7
2t (nm)	1.4
V_p (cm^3/g)	0.11

The second stage of weight loss (from about 400°C to 700°C) is also related to water molecules that are located between the layers of bentonite.

Also, in the study of polyacrylamide–polystyrene/bentonite nanocomposite thermal analysis diagram, about 70% weight loss at temperatures between 100°C and 700°C indicates the removal of water and the destruction of polymer chains between bentonite layers.

Therefore, polymer chains have been successfully placed at bentonite levels [44,45].

3.2. Adsorption

In this study, the results of the absorption of manganese ions from the aqueous solution by bentonite, polyacrylamide and nanocomposite polyacrylamide–polystyrene/bentonite absorbers were obtained and compared under optimal conditions.

To specify the optimal conditions:

Clause 1: first, with 10 g of adsorbent for 6 h, we measured the amount of solution adsorption containing 10 mg/L of manganese ions in the pH range of 2 to 7 to determine the optimum pH.

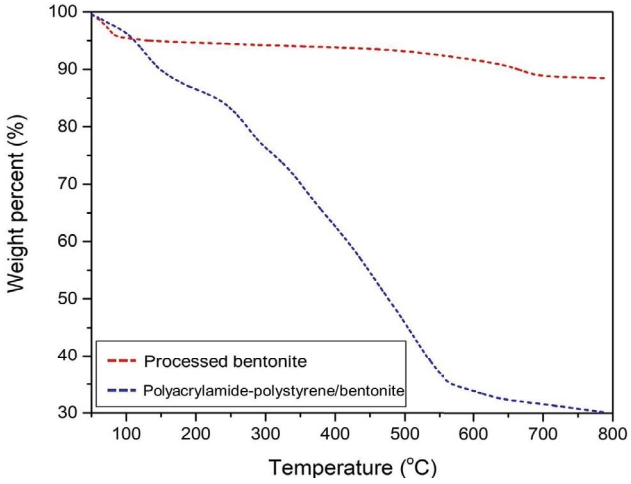

Fig. 9. Thermogravimetric analysis of processed bentonite and polyacrylamide–polystyrene/bentonite nanocomposite.

Clause 2: in the pH of the optimum obtained from the experiment of clause 1 in a period of 6 h, the amount of adsorption of the solution containing 10 mg/L of manganese ion was measured in the range of 5 to 15 g of adsorbent.

Clause 3: in the pH of the optimum and the adsorbent value of the optimum, the adsorption of the solution containing 10 mg/L of manganese ions in the range of 10 to 200 mg/L was measured.

3.2.1. pH effect on the metallic adsorption capacity

Changes in pH through the ionization degree of the adsorbent species affect adsorption because dual capacity metal ions can be present in aqueous solutions in various forms, including hydroxide compounds $M(OH)^+$, $M(OH)_2$, $M(OH)_3^-$. The most suitable species for adsorption on the desired adsorbent surface is M^{2+} species, which will be predominant for each cation at specific pH species. At higher pHs, the formation of metal hydroxides with simultaneous

adsorption process is effective in removing metal species from the solution.

In low pHs, competition between H^+ and M^{2+} reduces the adsorption capacity for the metal cation, and the disturbance of the H^+ species for the polymer bed, which occurs through the protonation of the O and N groups of the polymer, occupies the uptake positions of the cation-manganese uptake and reduces adsorption [46,47].

We performed the adsorption study by 10 g of adsorbent for 6 h to measure the amount of solution adsorption containing 10 mg/L of manganese ions in the pH range 2.0–7.0 (Table 2). Overall, nanocomposites have various advantages such as the high surface area, which may be attributed to the small particle size and the high number of active sites including the –OH functional group referred to the activation with HCl. These groups are helpful for the metal adsorption and elimination via the ion exchange or formation of metal complex mechanisms. Hence, the reactivity of the surface with –OH groups directly depends on the solution pH values. The metallic capacity values of manganese upgrade when the pH of the solution increases from pH 2.0 to 7.0 [48,49]. As mentioned, pH values affect adsorption by adsorbent manganese ion in aqueous solutions and manganese ion removal is enhanced as the pH value rises, reaching a maximum of around 6.

3.2.2. Effect of adsorbent dosage

To study the effect of the dosage on the removal efficiency of manganese ions, several studies were performed at pH = 6 (optimum pH), contact time of 6 h and concentration of manganese ions 10 mg/L with absorbent doses from 5 to 15 g.

Dosage is a crucial factor in the adsorption, since it assesses the adsorbent capacity for a special concentration of the metal ion solution. The amount of adsorbent is an important controlling parameter for the adsorption. Fig. 10 showed that the sorbent amount influences the removal processes of the divalent ionic manganese using PAA.B adsorbent, bentonite and polymer. In fact, when the sorbent dosage increased, the element capacity values of the divalent ionic manganese decreased from 5.0 to 15 g. This happens since the higher nanosorbent dosage results in more availability of exchangeable sites for the sorbate, exposing more active sites for binding with the divalent ionic manganese ions to the nanosorbent surface. Moreover, the metallic capacity enjoys high values in the presence of lower sorbent dosage because of an increased metal-to-sorbent ratio. Our objective in the low nanosorbent dosages was to examine the effect of the dosage on the efficiency of the manganese ions removal from the aqueous solutions based on different dosages of PAA.B nanocomposite, bentonite and polymer, as the removal of manganese ions grows when the PAA.B nanocomposite dosage rises due to the increase of the number of available adsorption sites for the adsorption [50].

3.2.3. Effect of contact time on the removal efficiency

The results of contact time on the removal efficiency are presented in Table 3.

The contact time is a significant parameter in adsorption capabilities. Generally, longer contact time can enhance the removal of pollutants, until an equilibrium state is achieved. The equilibrium may be achieved fast when the pollution concentration is low. The equilibrium time changes according to pollutant concentration in the solution. In fact, a longer contact time was effective to obtain greater removal efficiencies of manganese absorption which is a time-consuming process, and an increase in the contact time is beneficial for sufficient interactions between manganese and the adsorption sites of sorbents. The contact time for the adsorption of manganese by adsorbent was reported in a range of 2–24 h at the initial concentration of 10 mg/L, pH = 6 (optimum pH) and optimum dosage = 5 g. The maximum adsorption was obtained at 12 h. In the initial stage of the adsorption reaction, the adsorption sites on sorbents for manganese were sufficient. During time, more adsorption sites were occupied, and the adsorption capacity was eventually saturated. Hence, the optimum contact time was considered 12 h for manganese. Due to the availability and abundance of active sites on the adsorbent surface, the removal process was initially accelerated, but later, the number of active sites gradually reduced [51].

3.2.4. Effect of initial concentration

The effect of initial concentration on the removal efficiency and sorption capacity is demonstrated in Table 4.

To investigate the effect of the initial concentration, the adsorption of 10–200 mg L^{-1} of manganese from aqueous solution was examined at the optimum condition (dosage = 5 g, time = 12 h and pH = 6). However, at higher concentrations of manganese, the precipitation of manganese hydroxide may happen at pH 8.0 so the concentrations

Table 2
Effect of pH on adsorption of manganese ions from aqueous solution using (a) PAA.B nanocomposite, (b) bentonite, (c) polyacrylamide conditions: concentration of Mn ions (10 mg/L), adsorbent dosage (10 g), contact time (6 h)

pH	Polyacrylamide–polystyrene/ bentonite q_e (mg/g)	Bentonite q_e (mg/g)	Polyacrylamide q_e (mg/g)
2	1.7	0.8	0.44
3	2.8	1.3	0.72
4	3.7	1.8	0.98
5	4.6	2.3	1.3
6	5.3	2.7	1.6
7	5.2	2.6	1.55

above 200 mg L^{-1} were not applied. As can be seen in Table 4, the removal efficiency decreased as the initial concentration of manganese was elevated from 10 to 150 mg L^{-1}. This proves the high affinity of PAA for Mn(II). This little decrease in the removal efficiency can be explained by low initial concentration, the surface area and the relatively high accessibility of adsorption sites, so the manganese ions were easily adsorbed and removed. At higher initial concentrations, the total existing adsorption sites reduced as did the removal efficiency of manganese ions [52].

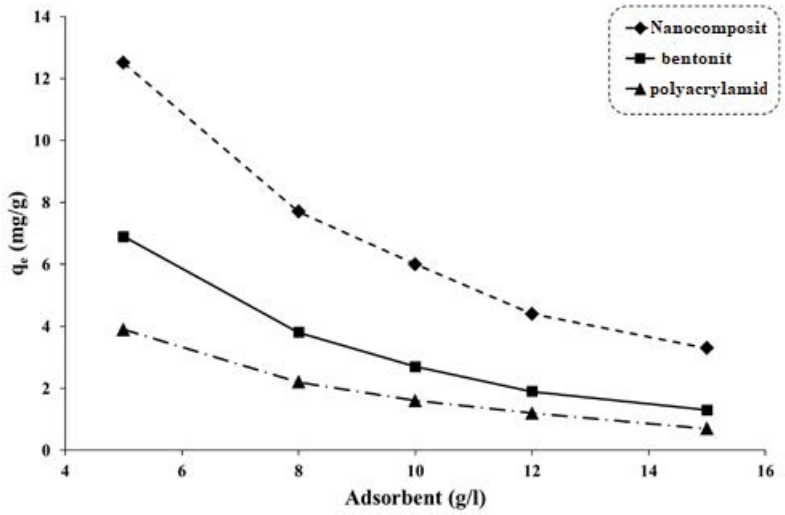

Fig. 10. Effect of adsorbent dosage on adsorption of manganese ions from aqueous solution using (a) PAA.B nanocomposite, and (b) bentonite, (c) polyacrylamide conditions: concentration of Mn ions (10 mg/L), pH (6), contact time (6 h).

Table 3
Effect of concentration of cation on adsorption of manganese ions from aqueous solution using (a) PAA.B nanocomposite, (b) bentonite, (c) polyacrylamide conditions: concentration of Mn ions (10 mg/L), adsorbent dosage (5 g), pH (6)

Contact time (h)	Polyacrylamide–polystyrene/ bentonite q_e (mg/g)	Bentonite q_e (mg/g)	Polyacrylamide q_e (mg/g)
2	6.2	3	1.7
4	9.7	4.9	2.8
6	12.5	6.2	3.5
8	13.9	7.1	4
12	15.4	7.9	4.4
24	15.35	7.85	4.35

Table 4
Effect of concentration cation on adsorption of manganese ions from aqueous solution using (a) PAA.B nanocomposite, (b) bentonite, (c) polyacrylamide conditions: contact time (12 h), adsorbent dosage (5 g), pH (6)

Concentration (mg/L)	Polyacrylamide-polystyrene/ bentonite q_e (mg/g)	Bentonite q_e (mg/g)	Polyacrylamide q_e (mg/g)
10	15.7	8.2	5.1
20	18.8	9.4	5.8
30	22.4	11.5	6.8
40	25.7	13.4	7.8
50	29.3	15.6	8.9
75	33.4	17.7	9.9
100	38.3	19.9	11
125	43.2	22.3	12
150	47.3	25	13.2
200	47.2	25.9	13.15

3.2.5. Reproducibility and retrieval

The results in Table 5 show the reproducibility and recovery of polyacrylamide–polystyrene/bentonite nanocomposite adsorbent in the adsorption of manganese ions from aqueous solution under optimal conditions.

Results of the manganese adsorption isotherms on PAA.B are shown in Figs. 11 and 12.

Adsorption isotherms are used to characterize the sorption technique and to evaluate the sorption capability.

Table 5
Reproducibility and retrieval

Retrieval	q_e (mg/g)
1	43.6
2	39
3	32.8
4	35.7
5	15.5
6	2.2

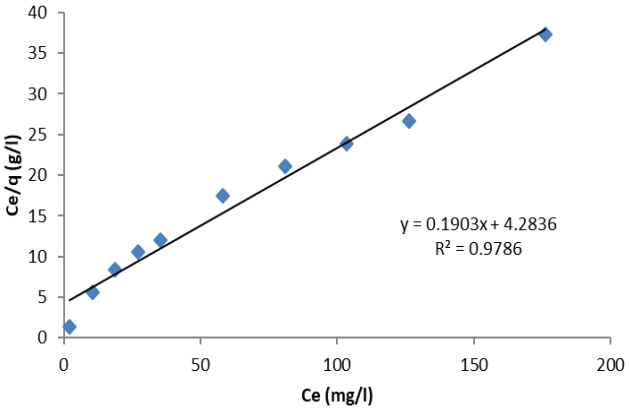

Fig. 11. Chart of Langmuir isotherm for adsorption of Mn(II) cations by adsorbent PAA.B nanocomposite.

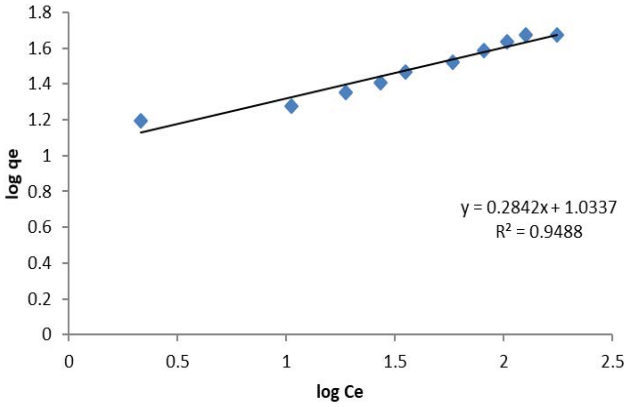

Fig. 12. Chart of Freundlich isotherm for adsorption of Mn(II) cations by adsorbent PAA.B nanocomposite.

Adsorption isotherm can be defined as the equilibrium correlation between the concentration in the adsorbent phase on the adsorbent elements and the concentration in the liquid phase. Some linear forms of these isotherms were used, which have a different axis. In such conditions, linear analysis is not so accurate and credible while nonlinear statistical functions are more precise. Recently, the nonlinear optimization modeling should be taken into more consideration as reported in recent studies on heavy metal adsorption.

In the different research on the uses of PAA.B for manganese adsorption, both Langmuir and Freundlich models have been used to analyze the adsorption data. However, most studies reported the Langmuir model as the better fit. The adsorption of manganese ion using PAA.B is usually a monolayer process happening on the surface, and in the model, the adsorption is considered to be a chemisorption process. In the Freundlich model, another significant adsorbent isotherm is appropriate for heterogeneous surfaces, widely applied to study the heavy metal adsorption. The model assumes the adsorption to be multilayer, indicating the heterogeneity of the surface of the adsorbent. While the adsorption of metal ions match better to either Freundlich or Langmuir isotherms, some adsorption processes are controlled by multiple mechanisms, hence, conforming well to both isotherms. However, compared with the regression correlation coefficients of the Freundlich model (R^2 = 0.9519), the Langmuir isotherm model (R^2 = 0.9786) matched with equilibrium data. This implied that there was monolayer adsorption on the structurally homogeneous nanofiber, all the adsorption sites were similar in terms of energy, and the adsorption mainly occurred at specific homogeneous sites.

Where q_e is the adsorption capacity at equilibrium (mg/g), C_e is the concentration of metal ion at equilibrium (ppm), and k_L are Langmuir constants referring to the maximum adsorption capacity (mg/g) and adsorption energy (L/mg), respectively. A dimensionless constant of R_L is a significant element of Langmuir isotherm which is defined in the following forms; C_0 and k_L are the highest initial ions concentration in ppm and Langmuir constant, respectively. The amount of R_L in the range of 0–1 reveals appropriateness of the adsorption process. The Freundlich model is formed based on the heterogeneous surface adsorption that assumes multilayer adsorption [53].

$$R_L = \frac{1}{1 + K_L C_0} \tag{14}$$

The value of R_L expresses the shape of the isotherm to be either unfavorable ($R_L > 1$), linear ($R_L = 1$), irreversible ($R_L = 0$) or favorable ($0 < R_L < 1$). Fig. 11 indicates that Langmuir isotherm is a better mathematical item for equilibrium data.

3.2.6. Batch adsorption kinetics

There was an accelerated adsorption of manganese on PAA.B and the adsorption steady state was obtained within 12 h. To obtain the adsorption equilibrium, a contact time of 24 h was chosen for the adsorption experiments. The kinetic studies of heavy metal adsorption onto PAA.B revealed

that the adsorption was carried out through a two-stage process. Large active sites on the surface of the adsorbent led to rapid uptake of the metal ions, but when the capacity of the active sites was going to end, the uptake was decelerated. The initial rapid stage occurs within a short time from the start of the process, while the second stage dominates the remaining part and is usually the rate-limiting step. To completely study the kinetics of the adsorption, kinetic data are fitted to various models such as pseudo-first-order, pseudo-second-order, etc. [54]. The relevant parameters obtained by linear fitting method are displayed in Figs. 12 and 13. As shown, pseudo-first-order (R^2 = 0.991) equations can thoroughly describe the experimental data, but pseudo-second-order (R^2 = 0.9894) may not describe the adsorption process satisfactorily. The relevant parameters obtained by the linear fitting method were displayed in Figs. 13 and 14. In general, the pseudo-first-order kinetics is more suitable to explain the initial stage of the adsorption. As shown, the pseudo-first-order kinetic equation was ideal to fit this whole process, indicating that the adsorption process of manganese onto nanocomposite was a diffusion-controlled process. The pseudo-second-order kinetic equation is based on the chemical reaction-controlled adsorption process, where the adsorbent and the adsorbate often share or exchange electrons to form a chemical covalent bond. The adsorption results shown in Figs. 12 and 13 indicate that the adsorption capacity of Mn(II) ion increased rapidly with time, and eventually reached a plateau. This can result from the several active sites on the surface area of the nanocomposite sorbent and better availability of the ion near the adsorbent at the initial stage of the adsorption process. These active sites were occupied by the adsorbate molecules during the time. The manganese ion adsorption capacities grew as the bentonite content of the nanocomposite sorbent increased. The maximum manganese ion adsorption was 7.85 mg g^{-1}, attained from PAA.B nanocomposite after 12 h.

3.2.7. Removal capability in real samples

Nano-composite polyacrylamide–polystyrene/bentonite adsorbent was used in the adsorption of manganese ions from the effluent of Mobarakeh Steel Company in Isfahan-Iran with a value of 8.3 mg/L. The result of using q_e = 6.24 mg/g and %Ads = 82.1% was determined.

Comparison of the results of adsorption percentage of manganese ions in optimal conditions by polyacrylamide–polystyrene/bentonite nanocomposite adsorbent (%Ads = 84.2) was compared with adsorbents involving carbon obtained from biomass (% Ads = 73), polyaniline nanocomposite (%Ads = 88) and SDS-Gutite (%Ads = 82) which indicates that the adsorbent presented in this work shows proper activity.

4. Conclusions

The adsorption process for the elimination of manganese ions was studied in detail. Adsorption is one of the most effective techniques for water treatment due to the flexibility and simplicity of design, reasonable cost, easy operation and insensitivity to toxic pollutants. The results indicated that PAA.B nanocomposite can be successfully used for the adsorption of manganese ions from aqueous solutions. It can be concluded that the process of adsorption of manganese ions on different adsorbents is attributed to the chemical nature of the adsorbents and different factors including solution pH, initial concentration, contact time and adsorbent dosage of the system. Low initial concentration resulted in lower removal efficiency; when the surface area and the accessibility of adsorption sites were fairly high, the manganese ions could easily be adsorbed and removed. At higher initial concentrations, the total existing adsorption sites reduced, causing lower removal efficiency of manganese ions. With higher initial concentration of solution, q_e increases because of enhanced driving force at higher equilibrium concentrations. Kinetics of manganese on PAA.B nanocomposites adheres to the pseudo-first-order model. Study of adsorption isotherm showed that Langmuir model was an appropriate model in adjusting the adsorption process.

Acknowledgments

The authors thank the member of chemistry and agricultural laboratory of Islamic Azad University, Ahvaz and Shahreza Branch for helpful contribution. The authors would also like to thank the above universities for the financial support provided.

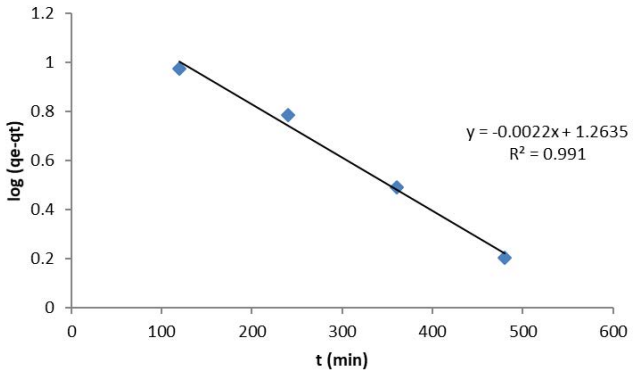

Fig. 13. Pseudo-first-order kinetics in adsorption of Mn(II) cations by PAA.B nanocomposite.

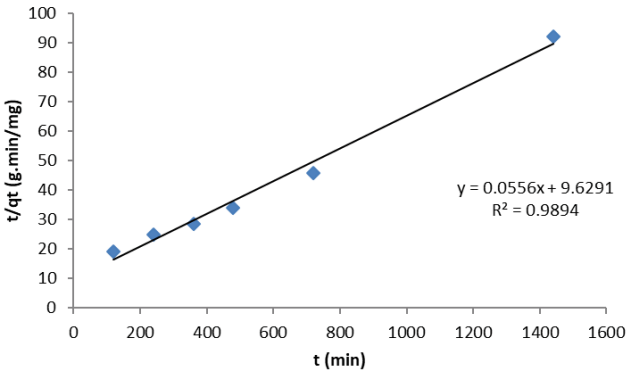

Fig. 14. Pseudo-second-order kinetics in adsorption of Mn(II) cations by PAA.B nanocomposite.

References

[1] M.K. Uddin, A review on the adsorption of heavy metals by clay minerals, with special focus on the past decade, Chem. Eng. J., 308 (2017) 438–462.

[2] W. Dong, Y. Zhang, X. Quan, Health risk assessment of heavy metals and pesticides: a case study in the main drinking water source in Dalian, China, Chemosphere, 242 (2020) 125113.

[3] A. Azimi, A. Azari, M. Rezakazemi, M. Ansarpour, Removal of heavy metals from industrial wastewaters: a review, ChemBioEng Rev., 4 (2017) 37–59.

[4] M.R. Miah, O.M. Ijomone, C.O.A. Okoh, O.K. Ijomone, G.T. Akingbade, T. Ke, B. Krum, A. C. Martins Jr., A. Akinyemi, N. Aranoff, F.A. A. Soares, A.B. Bowman, M. Aschner, The effects of manganese overexposure on brain health, Neurochem. Int., 135 (2020) 104688.

[5] A. Wennberg, A. Iregren, G. Struwe, G. Cizinsky, M. Haqrnan, L. Johansson, Manganese exposure in steel smelters a health hazard to the nervous system, Scand. J. Work Environ. Health, 17 (1991) 255–262.

[6] B. Tang, P. Tong, K.S. Xue, P.L. Williams, J.S. Wang, L. Tang, High-throughput assessment of toxic effects of metal mixtures of cadmium(Cd), lead(Pb), and manganese(Mn) in nematode *Caenorhabditis elegans*, Chemosphere, 234 (2019) 232–241.

[7] R. Zhang, X. Ma, X. Shen, Y. Zhai, T. Zhang, C. Ji, J. Hong, Life cycle assessment of electrolytic manganese metal production, J. Cleaner Prod., 253 (2020) 119951.

[8] M.K. Kumari, D. Varaprasad, D. Narasimham, K. Paramesh, T. Chandrasekhar, Impacts of cadmium and manganese on in vitro seed germination and seedling growth of horsegram, Indian J. Plant Sci., 5 (2016) 119–125.

[9] Y. Li, H. Huang, Z. Xu, H. Ma, Y. Guo, Mechanism study on manganese(II) removal from acid mine wastewater using red mud and its application to a lab-scale column, J. Cleaner Prod., 253 (2020) 119955.

[10] M.K. Doula, Removal of Mn^{2+} ions from drinking water by using Clinoptilolite and a Clinoptilolite–Fe oxide system, Water Res., 40 (2006) 3167–3176.

[11] M.H. Qomi, H. Eisazadeh, M. Hosseini, H.A. Namaghi, Manganese removal from aqueous media using polyaniline nanocomposite coated on wood sawdust, Synth. Metals, 194 (2014) 153–159.

[12] M.S. Islam, M.S. Rahaman, J.H. Yeum, Phosphine-functionalized electro spun poly (vinyl alcohol)/silica nanofibers as highly effective adsorbent for removal of aqueous manganese and nickel ions, Colloids Surf. A, 484 (2015) 9–18.

[13] A.A. Bakr, N.A. Sayed, T.M. Salama, I.O. Ali, R.R. Abdel Gayed, N.A. Negm, Kinetics and thermodynamics of Mn(II) removal from aqueous solutions onto Mg-Zn-Al LDH/montmorillonite nanocomposite, Egypt. J. Pet., 27 (2018) 1215–1220.

[14] K. Tohdee, L. Kaewsichan, Asadulla, Enhancement of adsorption efficiency of heavy metal Cu(II) and Zn(II) onto cationic surfactant modified bentonite, J. Environ. Chem. Eng., 6 (2018) 2821–2828.

[15] G. Zhao, H. Zhang, Q. Fan, X. Ren, J. Li, Y. Chen, X. Wang, Sorption of copper(II) onto super-adsorbent of bentonite–polyacrylamide composites, J. Hazard. Mater., 173 (2010) 661–668.

[16] S. Wijeratne, M.L. Bruening, G.L. Baker, Layer-by-layer assembly of thick, Cu^{2+}-chelating films, Langmuir, 29 (2013) 12720–12729.

[17] A.A. Baker, M.A. Betiha, A.H. Mady, M.F. Menoufy, S.M. Dessouky, Removal of manganese ions from their aqueous solutions by organophilic montmorillonite (OMMT), Water Treat., 57 (2016) 19519–19528.

[18] T.S. Anirudhan, P.S. Suchithra, S. Rijith, Amine–modified polyacrylamide-bentonite composite for the adsorption of humic acid in aqueous solutions, Colloids Surf. A, 326 (2008) 147–156.

[19] H.G. Seong, J. Ryu, Y. Qian, J. So, S.H. Baeck, S.E. Shim, Novel hierarchically porous melamine-vanillin polymer: synthesis and application for the Pb(II) ion removal in wastewater, Macromol. Res., 27 (2019) 882–887.

[20] J. Cao, Y. Tan, Y. Che, H. Xin, Novel complex gel beads composed of hydrolyzed polyacrylamide and chitosan: an effective adsorbent for the removal of heavy metal from aqueous solution, Bioresour. Technol., 101 (2010) 2558–2561.

[21] X. Zheng, H. Zheng, Z. Xiong, R. Zhao, Y. Liu, C. Zhao, C. Zheng, Novel anionic polyacrylamide-modify-chitosan magnetic composite nanoparticles with excellent adsorption capacity for cationic dyes and pH-independent adsorption capability for metal ions, Chem. Eng. J., 392 (2020) 123706.

[22] S. Moulay, N. Bensacia, F. Garin, I. Fechete, A. Boos, Synthesis of polyacrylamide-bound hydroquinone via a homolytic pathway: application to the removal of heavy metals, C.R. Chimie, 17 (2014) 849–859.

[23] H. Kasgoz, S. Ozgumus, M. Orbay, Modified polyacrylamide hydrogels and their application in removal of heavy metal ions, Polymer, 44 (2003) 1785–1793.

[24] H. Zhu, X. Xiao, Z. Guo, X. Han, Y. Liang, Y. Zhang, C. Zhou, Adsorption of vanadium(V) on natural kaolinite and montmorillonite: characteristics and mechanism, Appl. Clay Sci., 161 (2018) 310–316.

[25] S. Mnasri-Ghnimi, N. Frini-Srasra, Removal of heavy metals from aqueous solutions by adsorption using single and mixed pillared clays, Appl. Clay Sci., 179 (2019) 105151.

[26] J.D. Castro-Castro, N.R. Sanabria-Gonzalez, G.I. Giraldo-Gomez, Experimental data of adsorption of Cr(III) from aqueous solution using a bentonite: optimization by response surface methodology, Data Brief, 28 (2020) 105022.

[27] S.K. Singh, K.Y. Rhee, S.Y. Lee, S.J. Park, Facile fabrication of poly(vinyl alcohol)/silica composites for removal of Hg(II) from water, Macromol. Res., 23 (2015) 21–29.

[28] H. Javadian, Adsorption performance of suitable nanostructured novel composite adsorbent of poly(N-methylaniline) for removal of heavy metal from aqueous solutions, J. Ind. Eng. Chem., 20 (2014) 4344–4352.

[29] Y. Wu, J. Zhou, Y, Wen, L. Jiang, Y. Wu, Biosorption of heavy metal ions (Cu^{2+}, Mn^{2+}, Zn^{2+}, and Fe^{3+}) from aqueous solutions using activated sludge: comparison of aerobic activated sludge with anaerobic activated sludge, Appl. Biochem. Biotechnol., 168 (2012) 2079–2093.

[30] C.S.C. Chiew, H.K. Yeoh, P. Pasbakhsh, K. Krishnaiah, P.E. Poh, B.T. Tey, E.S. Chan, Halloysite/alginate nanocomposite beads: kinetics, equilibrium and mechanism for lead adsorption, Appl. Clay Sci., 119 (2016) 301–310.

[31] T. Apiradee, A. Ornanong, S. Ponlayuth, J. Sorapong, N. Wimol, Adsorption isotherm models and error analysis for single and binary adsorption of Cd(II) and Zn(II) using leonardite as adsorbent, Environ. Earth Sci., 7 (2017) 777.

[32] N. Ballav, H.J. Choi, S.B. Mishra, A. Maity, Synthesis, characterization of Fe_3O_4@glycine doped polypyrrole magnetic nanocomposites and their potential performance to remove toxic Cr(VI), J. Ind. Eng. Chem., 20 (2014) 4085–4093.

[33] Z. Lou, W. Zhang, X. Hu, H. Zhang, Synthesis of a novel functional group-bridged magnetized bentonite adsorbent: characterization, kinetics, isotherm, thermodynamics and regeneration, J. Chem. Eng., 25 (2017) 587–594.

[34] P. Ganesan, R. Kamaraj, G. Sozhan, S. Vasudevan, Oxidized multiwalled carbon nanotubes as adsorbent for the removal of manganese from aqueous solution, Environ. Sci. Pollut. Res., 20 (2013) 987–996.

[35] M. Anbia, S. Amirmahmoodi, Removal of Hg(II) and Mn(II) from aqueous solution using nanoporous carbon impregnated with surfactants, Arabian J. Chem., 9 (2016) S319–S325.

[36] M.D.L. Balela, N.M. Intila, S.R. Salvanera, Adsorptive removal of lead ions in aqueous solution by Kapok-polyacrylonitrile nanocomposites, Mater. Today, 17 (2019) 672–678.

[37] F.S. Hashem, M.S. Amin, S.M.A. El-Gamal, Chemical activation of vermiculite to produce highly efficient material for Pb^{2+} and Cd^{2+} removal, Appl. Clay Sci., 115 (2015) 189–200.

[38] M. Asgari, A. Abouelmagd, U. Sundararaj, Silane functionalization of sodium montmorillonite nanoclay and its effect on rheological and mechanical properties of HDPE/clay nanocomposites, Appl. Clay Sci., 146 (2017) 439–448.

[39] L.T.M. Thy, N.H. Kiem, T.H. Tu, L.M. Phu, D.T.Y. Oanh, H.M. Nam, M.T. Phong, N.H. Hieu, Fabrication of manganese ferrite/graphene oxide nanocomposites for removal of nickel ions, methylene blue from water, Chem. Phys., 533 (2020) 110700.
[40] F. Ge, M.M. Li, H. Ye, B.X. Zhao, Effective removal of heavy metal ions Cd^{2+}, Zn^{2+}, Pb^{2+}, Cu^{2+} from aqueous solution by polymer-modified magnetic nanoparticles, J. Hazard. Mater., 211–212 (2012) 366–372.
[42] L. Xia, Y. Lu, H. Meng, C. Li, Preparation of C-MOx nanocomposite for efficient absorption of heavy metal ions via mechanochemical reaction of CaC_2 and transitional metal oxides, J. Hazard. Mater., 393 (2020) 122487.
[42] U. Kamran, Y.J. Heo, J.W. Lee, S.J. Park, Chemically modified activated carbon decorated with MnO_2 nanocomposites for improving lithium adsorption and recovery from aqueous media, J. Alloys Compd., 794 (2019) 425–434.
[43] K.S. Walton, R.Q. Snurr, Applicability of the BET method for determining surface areas of microporous metal–organic frameworks, J. Am. Chem. Soc., 129 (2007) 8552–8556.
[44] G. Wang, S. Wang, W. Sun, Z. Sun, S. Zheng, Synthesis of a novel illite@carbon nanocomposite adsorbent for removal of Cr(VI) from wastewater, J. Environ. Sci., 57 (2017) 62–71.
[45] M. Jesús Fernández, M. Dolores Fernández, A. Ibai, Poly (l-lactic acid)/organically modified vermiculite nanocomposites prepared by melt compounding: effect of clay modification on microstructure and thermal properties, Eur. Polym. J., 49 (2013) 1257–1267.
[46] N. Rajic, D. Stojakovic, S. Jevtic, N.Z. Logar, J. Kovac, V. Kaucic, Removal of aqueous manganese using the natural zeolitic tuff from the Vranjska Banja deposit in Serbia, J. Hazard. Mater., 172 (2009) 1450–1457.
[47] W. Wang, X. Zhang, H. Wang, X. Wang, L. Zhou, R. Liu, Y. Liang, Laboratory study on the adsorption of Mn2D on suspended and deposited amorphous $Al(OH)_3$ in drinking water distribution systems, Water Res., 46 (2012) 4063–4070.
[48] S.R. Taffarel, J. Rubio, On the removal of Mn^{2+} ions by adsorption onto natural and activated Chilean zeolites, Miner. Eng., 22 (2009) 336–343.
[49] L. Ma, Y. Peng, B. Wua, D. Lei, H. Xu, *Pleurotus ostreatus* nanoparticles as a new nano-biosorbent for removal of Mn(II) from aqueous solution, Chem. Eng. J., 225 (2013) 59–67.
[50] L. Zeng, Y. Chen, Q. Zhang, X. Guo, Y. Peng, H. Xiao, X. Chen, J. Luo, Adsorption of Cd(II), Cu(II) and Ni(II) ions by cross-linking chitosan/rectorite nano-hybrid composite microspheres, Polymers, 130 (2015) 333–343.
[51] T.S. Anirudhan, P.S. Suchithra, Humic acid-immobilized polymer/bentonite composite as an adsorbent for the removal of copper(II) ions from aqueous solutions and electroplating industry wastewater, J. Ind. Eng. Chem., 16 (2010) 130–139.
[52] Z. Hongxia, W. Xiaoyun, L. Honghong, T. Tianshe, W. Wangsuo, Adsorption behavior of Th(IV) onto illite: effect of contact time, pH value, ionic strength, humic acid and temperature, Appl. Clay Sci., 127–128 (2016) 35–43.
[53] G. Moradi, F. Dabirian, P. Mohammadi, L. Rajabi, M. Babaei, N. Shiri, Electrospun fumarate ferroxane/polyacrylonitrile nanocomposite nanofibers adsorbent for lead removal from aqueous solution: characterization and process optimization by response surface methodology, Chem. Eng. Res. Des., 129 (2018) 182–196.
[54] S. Malamis, E. Katsou, A review on zinc and nickel adsorption on natural and modified zeolite, bentonite and vermiculite: examination of process parameters, kinetics and isotherms, J. Hazard. Mater., 252–253 (2013) 428–461.
[55] W. Jiang, X. Chen, B. Pan, Q. Zhang, L. Teng, Y. Chen, L. Liu, Spherical polystyrene-supported chitosan thin film of fast kinetics and high capacity for copper removal, J. Hazard. Mater., 276 (2014) 295–301.
[56] D. Savova, N. Petrov, M.F. Yardim, E. Ekinci, T. Budinova, M. Razvigorova, V. Minkova, The influence of the texture and surface properties of carbon adsorbents obtained from biomass products on the adsorption of manganese ions from aqueous solution, Carbon, 41 (2003) 1897–1903.
[57] M. Hallajiqomi, H. Eisazadeh, Adsorption of manganese ion using polyaniline and it's nanocomposite: kinetics and isotherm studies, J. Ind. Eng. Chem., 55 (2017) 191–197.
[58] R. Mohammed, H.H. El-Maghrabi, A.A. Younes, A.B. Farag, S. Mikhail, M. Riad, SDS-goethite adsorbent material preparation, structural characterization and the kinetics of the manganese adsorption, J. Mol. Liq., 231 (2017) 499–508.